Available online at www.sciencedirect.com
ScienceDirect
Journal of the European Ceramic Society 27 (2007) 3971–3976
www.elsevier.com/locate/jeurceramsoc

# Structure and dielectric properties of $Ln_3NbO_7$ (Ln = Nd, Gd, Dy, Er, Yb and Y)

Lu Cai, Juan C. Nino *

*Department of Materials Science and Engineering, University of Florida, Gainesville, Florida 32611, United States*

Available online 29 March 2007

**Abstract**

The structure and dielectric properties of $Ln_3NbO_7$ (Ln = Nd, Gd, Dy, Er, Yb and Y) ceramics are investigated. With decreasing ionic radius of $Ln^{3+}$, the stable crystal structure of the compounds shifts from orthorhombic weberite to defect fluorite. It is experimentally observed that, with the exception of $Gd_3NbO_7$, the room temperature real part of the relative permittivity of $Ln_3NbO_7$ ceramics decreases from approximately 40 to 30 (at 1 MHz) with increasing ionic radius of $Ln^{3+}$. The observed imaginary part of the relative permittivity is in order of $10^{-2}$ to $10^{-1}$ (room temperature and 1 MHz) and it is relatively stable up to 80 °C, where it increases with a rise in temperature. Interesting exceptions of these trends are $Nd_3NbO_7$ that crystallizes with a weberite-type structure and shows large positive temperature variation of the dielectric properties, and $Gd_3NbO_7$ that crystallized in a weberite related structure and displays frequency and temperature dependent dielectric relaxation behavior.


*Keywords:* Dielectric properties; Relaxation

## 1. Introduction

Oxide pyrochlore compounds with $A_2B_2O_7$ stoichiometry (where A and B are metals or transition metals) exhibit interesting dielectric properties with intermediate dielectric constants especially in niobates, tantalates and titanates ($\varepsilon_r \sim 30$–$100$).[1] Previous theoretical and experimental investigations aimed at expanding the family of pyrochlore dielectrics have predicted and demonstrated the existence of $Ln_2(B',B'')_2O_7$ compounds, where B″ include Nb and Ta.[2] Of great crystallochemical interest is the possibility of forming $(Ln1)_2(Ln2,Nb)O_7$ compounds (where Ln = lanthanide) with the pyrochlore crystal structure. In particular, to date reports on the crystal structure of compounds within the $Ln_3NbO_7$ series (Ln1 = Ln2) are contradictory. For example, $Sm_3NbO_7$ and $Gd_3NbO_7$ have been reported as orthorhombic with a weberite-type structure, while others have reported the compounds as pyrochlores.[3–8] In other cases, a cubic defect fluorite-type or pyrochlore-type structure has been reported for $Ln_3NbO_7$ compounds, in which the ionic radius of $Ln^{3+}$ cation was equal to or less than that of $Dy^{3+}$.[3–6,8] In addition, based on electron diffraction investigations, it has been proposed that microdomains of an undermined fluorite-related superstructure exist within these compounds.[5] From Raman spectroscopy studies, Kovyazina et al.[9] proposed $Y_3NbO_7$ as a "domain pyrochlore" structure, in which the oxygen vacancies are ordered in the same way as in a pyrochlore structure but only at a local (domain) level. This local order was also proposed as an explanation of the non-ideal pyrochlore X-ray diffraction (XRD) profile observed.[9] Finally, an orthorhombic weberite-type structure with space group *Cmcm* has been reported for $Ln_3NbO_7$ (Ln = $La^{3+}$, $Pr^{3+}$ and $Nd^{3+}$).[3–8,10]

Some insight on this discrepancy regarding the crystal structure reported for these compounds can be obtained by contrasting the different crystal structures proposed. Weberites and pyrochlores, expressed as $A_2B_2O_7$, can be seen as anion deficient superstructure derivatives of the fluorite structure ($MO_2$). The reduction in the number of anions leads to a decrease in the coordination number of B cations (VI coordination) with respect to the A cations (VIII coordination) and introduces variation in the cation valence to keep the compound neutral.[11] In the weberite structure there are equal number of VI and VIII coordinated cations in an ordered $BO_6$–$AO_8$ layer arrangement. By contrast, even though the $Ln_3NbO_7$ compounds tend to crystallize in an arrangement of $NbO_6$–$LnO_8$ layers (much like weberites), a different cation configuration between the layers leads VII coordination (Fig. 1). As such, pyrochlores can be seen

* Corresponding author. Tel.: +1 352 8463787; fax: +1 352 8463355.
*E-mail address:* jnino@mse.ufl.edu (J.C. Nino).

0955-2219/$ – see front matter © 2007 Elsevier Ltd. All rights reserved.
doi:10.1016/j.jeurceramsoc.2007.02.077

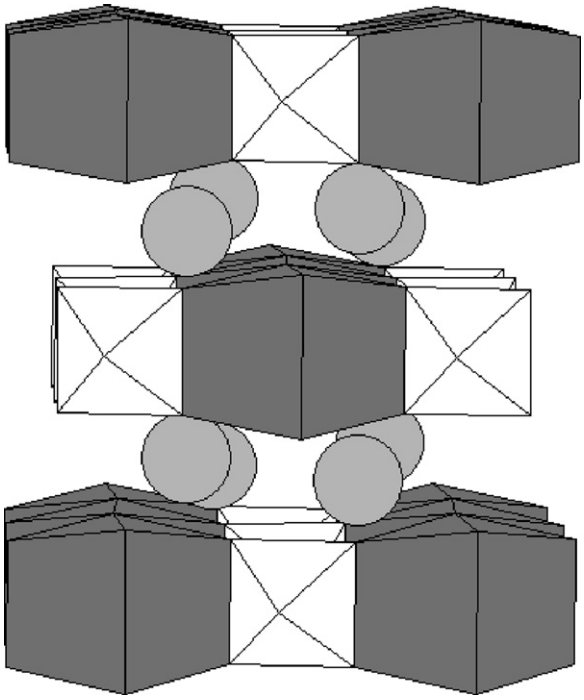

Fig. 1. Weberite-type structure of $Ln_3NbO_7$ (based on atomic positions after Rosell[4]). The circles show VII coordinated $Ln^{3+}$. The grey polyhedron show $LnO_8$ cubes and the white ones indicate $NbO_6$ octahedra.

as an intermediate between fluorite and weberite structures.[11] Further, since rare earth elements show a nearly linear relationship between the ionic radius and polarizability,[12,13] the series of $Ln_3NbO_7$ compounds provides an interesting stage for studying the structure–dielectric properties relationships, as well as correlations among ionic radii, ion polarizability within fluorite-related structures.

It is important to note, that the dielectric properties of some compounds within the $Ln_3NbO_7$ series were previously investigated by Chinchol[14] on the $xSm_3NbO_7 + (1-x)La_3NbO_7$ system and by Astafyev et al.[15] on the $Ln_3NbO_7$ (Ln = Sm–Gd) system; both studies limited to 1 kHz. However, to explore the fundamental structure–dielectric properties relationships, in the present work, research was conducted on the dielectric properties of $Ln_3NbO_7$ (Ln = Nd, Gd, Dy, Er, Yb and Y) over a broad range of frequency and temperature.

## 2. Experimental procedure

Polycrystalline specimens were prepared by conventional solid-state processing. The starting materials were $Dy_2O_3$ (Alfa, 99.99%), $Er_2O_3$ (Alfa, 99.99%), $Nd_2O_3$ (Alfa, 99.9%), $Y_2O_3$ (ACROS, 99.99%), $Yb_2O_3$ (Alfa, 99.9%) and $Nb_2O_5$ (Alfa, 99.9985%). Molar ratios of 3:1 $Ln_2O_3$ and $Nb_2O_5$ were combined with 70 ml deionized water and 2 ml ammonium polyacrylate dispersant (Darvan 821 A). The slurry was ball-milled for 24 h, subsequently dried in the oven at 120 °C for 16 h, then ground and sieved through a 212 μm mesh. The powder was then placed in an alumina crucible and calcined at 1300–1400 °C for 6–8 h. X-ray diffraction was performed to confirm phase formation using Cu Kα radiation at room temperature.

After calcination, 1–3 wt.% of PVA binder (Celvol 103) was added to assist in pellet formation. Pellets were uniaxially pressed, at 150 MPa, into cylindrical pellets, 13 or 7 mm in diameter and approximately 1.5 mm thick. Pellets were sintered at 1650 °C for 4 h following a binder burn-out step added at 450 °C for 2 h. The density of every pellet was above 92% of the theoretical density. For dielectric measurements parallel plate capacitors were made by sputtering Au/Pd electrodes on both sides of pellets followed by a painted coat of air-dried Ag paste.

## 3. Results and discussion

### 3.1. Crystal structure

The XRD profile of $Nd_3NbO_7$ is shown in Fig. 2. The experimental pattern of $Nd_3NbO_7$ is in excellent agreement with the theoretical XRD pattern based on the atomic positions after Rossell.[4] While all the experimentally observed peaks are part of the $Nd_3NbO_7$ crystal structure, only the peaks with relative intensities larger than 8% are indexed in Fig. 2, while the less intense peaks are indicated by diamond symbols.

The XRD patterns for $Gd_3NbO_7$ and $Dy_3NbO_7$ are shown in Fig. 3. At first glance, both spectra match well a cubic fluorite profile. However, the $Gd_3NbO_7$ pattern contains more minor peaks with intensities below 5% of the relative intensity. These minor peaks have been identified in the past as superlattice lines typically associated with pyrochlore structure by Abe et al.[8] However, that claim was not based on detailed XRD analysis. Based on the $Gd_3NbO_7$ XRD profile here collected, some of the peaks cannot be attributed to the pyrochlore structure. These peaks are indexed as the planes with mixed odd and even of *h*, *k*, *l* values, and they violate the reflection condition for pyrochlore in which *h*, *k*, *l* values should be either all odd or all even. By contrast, all of the peaks can be correctly indexed on the basis of the $Gd_3TaO_7$ compound (JCPDS 38-1409), which according to Yokogawa et al.[16] is a weberite-type structure with space group $C222_1$. The theoretical XRD profile using Pseudo-Voigt

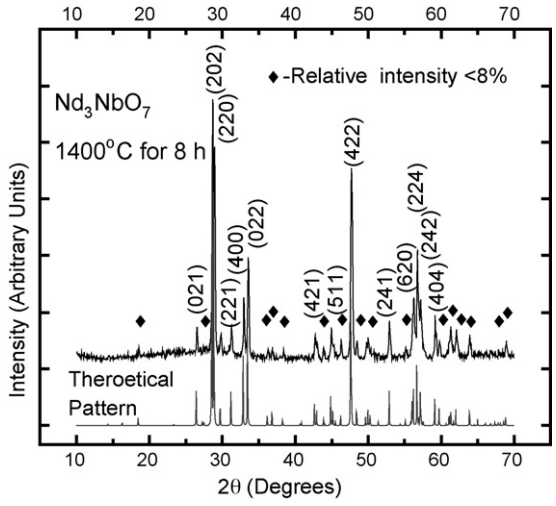


Fig. 2. Experimental and theoretical XRD of $Nd_3NbO_7$[4].

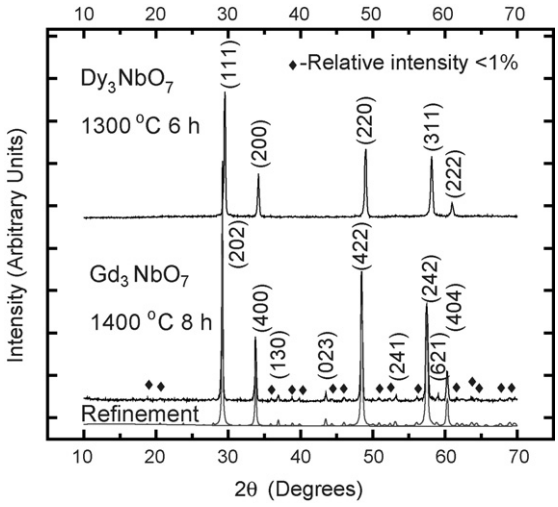


Fig. 3. XRD of $Gd_3NbO_7$ (both experimental profile and refinement) and $Dy_3NbO_7$.

peak profile function on the basis of space group $C222_1$ is also shown in Fig. 3 for comparison. Further proof for this crystallographic assignment has been obtained in the past by Raman spectroscopy, also pointing to $Gd_3NbO_7$ as a weberite related structure.[9] The peaks with relative intensities larger than 1% are indexed and others are indicated by diamond symbols in Fig. 3.

The XRD spectra of $Ln_3NbO_7$ (Ln = Er, Yb and Y) are almost identical to that of $Dy_3NbO_7$. As expected, there is a shift in $2\theta$ values indicating changes in the lattice parameter. The XRD profiles for these four compounds are all consistent with a cubic fluorite structure and show no reflections associated with the pyrochlore structure. However, according to Raman spectroscopy analysis by Kovyazina et al.[9], $Y_3NbO_7$ shows the six characteristic active Raman spectroscopy lines ($A_{1g}$,$E_g$,$4F_{2g}$) for the pyrochlore structure. It is quite possible then that the same local ordering is occurring in other $Ln_3NbO_7$ (Ln = Dy, Er and Yb) compounds. While detailed Raman spectroscopy analysis of these compounds is ongoing and will be matter of future publications, these compounds are considered to be ordered defect fluorites for the purpose of the present investigation. The lattice parameters listed in Table 1 are calculated using refinement routines in Powdercell crystallographic software for the orthorhombic structures as well as the Nelson–Riley function for the cubic structures.

Table 1
Lattice parameters of $Ln_3NbO_7$ (Ln = Nd, Gd, Dy, Er, Yb, Y)

| Compound | *a* (Å) | *b* (Å) | *c* (Å) |
|---|---|---|---|
| $Nd_3NbO_7$ | 10.9185[a] | 7.5365 | 7.6369 |
| $Gd_3NbO_7$ | 10.6309 | 7.5375 | 7.5454 |
| $Dy_3NbO_7$ | 5.2701 (5)[b] | | |
| $Er_3NbO_7$ | 5.2318 (7) | | |
| $Yb_3NbO_7$ | 5.1944 (10) | | |
| $Y_3NbO_7$ | 5.2534 (6) | | |

[a] The standard limits for deviations are 0.1%.
[b] Numbers in parentheses are standard deviations.

### 3.2. Microstructure

The representative microstructures of the $Yb_3NbO_7$ and $Gd_3NbO_7$ pellets sintered at 1650 °C for 4 h are presented in Fig. 4. The SEM images of the other $Ln_3NbO_7$ (Ln = Nd, Dy, Er, Yb and Y) pellets are nearly the same as $Yb_3NbO_7$. $Yb_3NbO_7$ has larger average grain size and broader grain size distribution than that of $Gd_3NbO_7$. Limited closed porosity is also observed at the grain boundaries. As mentioned before, the porosity of all the synthesized compounds are below 8%.

### 3.3. Dielectric properties

Fig. 5 shows the dielectric properties for $Nd_3NbO_7$ as a function of temperature at different frequencies from1 kHz to 1 MHz. The real part of permittivity increases from 33 to 62 between −160 °C and 200 °C. The variation of the real part of permittivity with frequency is negligible at low temperatures. However, at higher temperatures (approximately from 80 °C), frequency dispersion in the real part of the relative permittivity occurs, accompanied by a sharp increase in the imaginary part of the relative permittivity at 1 kHz (∼13.6 at 200 °C). This behavior is consistent with the onset of electrical conduction within the sample. However, before this phenomenon, the large positive temperature coefficient of the real part of the relative permittivity ($1.7 \times 10^3$ ppm/°C between −55 °C and 125 °C) may be

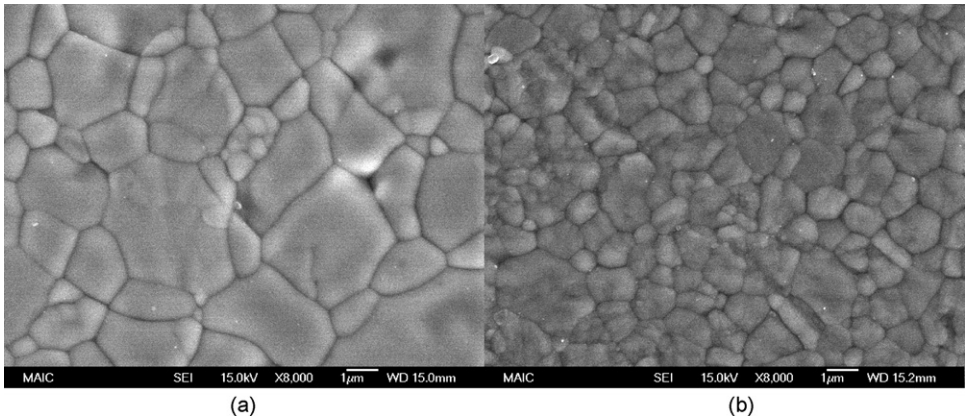


Fig. 4. SEM pictures of $Ln_3NbO_7$ pellets sintered at 1650 °C for 4 h: (a) $Yb_3NbO_7$ and (b) $Gd_3NbO_7$.

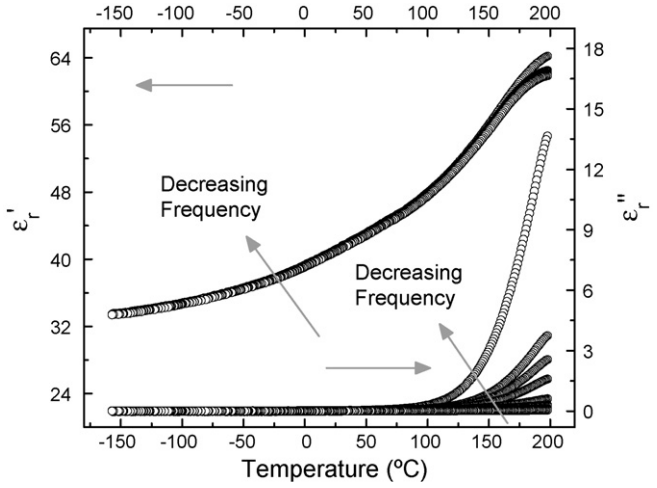


Fig. 5. Real and imaginary parts of the relative permittivity of $Nd_3NbO_7$ at 1 kHz, 4 kHz, 6 kHz, 10 kHz, 30 kHz, 80 kHz, 100 kHz, 300 kHz, 800 kHz and 1 MHz.

indicative of a high temperature phase transformation that is obscured by the conductivity.

The dielectric behavior of $Gd_3NbO_7$ as a function of temperature at the frequencies from 1 kHz to 1 MHz is shown in Fig. 6. The real part of permittivity is between 34 and 48, and the imaginary part of permittivity is on the order of $10^{-4}$ to $10^{-1}$ at 1 MHz from −160 °C to 200 °C. It is observed that the dielectric response undergoes a frequency and temperature dependent dielectric relaxation behavior. Compared to the $Nd_3NbO_7$ structure, the structure of $Gd_3NbO_7$ has largely distorted $LnO_8$ cubes and $NbO_6$ octahedra.[4,17] Therefore, these distortions may be responsible for the different dielectric responses of these two weberite-type structures. The real part of the relative permittivity of $Gd_3NbO_7$ at different frequencies becomes more dispersive with rising temperature, increasing sharply from −160 °C to approximately 50 °C where a maximum is reached. At higher temperatures the real part of the relative permittivity decreases slightly with increasing temperature. The temperature, at which the peak of the imaginary part occurs, shifts to higher temperatures with increasing frequency. That being the case, it is unclear

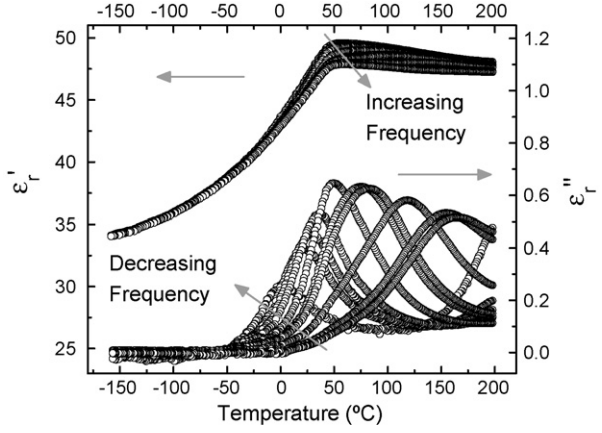


Fig. 6. Real and imaginary parts of the relative permittivity of $Gd_3NbO_7$ at 1 kHz, 4 kHz, 6kHz, 10 kHz, 30 kHz, 80 kHz, 100 kHz, 300 kHz, 800 kHz and 1 MHz.

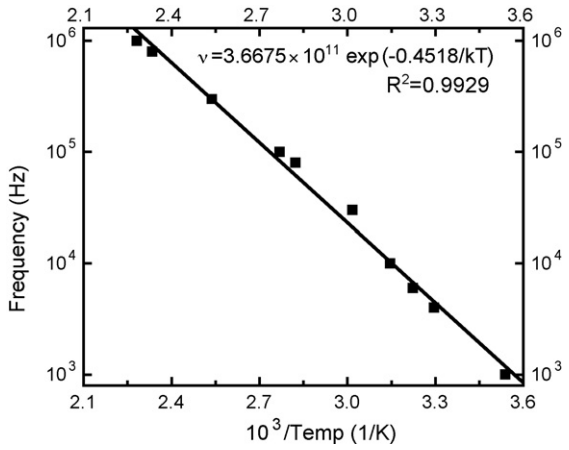


Fig. 7. Arrhenius plot of temperature at which the maximum loss peak occurs in $Gd_3NbO_7$.

why there is no clear shift in the maxima of the real part of the relative permittivity. To better understand the phenomena, the Arrhenius function is used to model the relaxation behavior of $Gd_3NbO_7$:

$$v = v_0 \exp\left[-\frac{E_a}{k_B T_m}\right] \quad (1)$$

where $v$ is the measuring frequency, the pre-exponential $v_0$ the attempt jump frequency, $E_a$ the activation energy and $k_B$ is the Boltzmann's constant. The resulting Arrhenius plot is presented in Fig. 7. From the linear fit, $v_0 = 3.6675 \times 10^{11}$ Hz, and the activation energy $E_a$ is 0.4518 eV, which is larger than typical values observed in dielectric glasses and relaxor ferroelectrics.[18,19] However, other ionic and dipolar compounds systems have even higher activation energies; for example, 0.53 eV for $CaF_2$ doped NaF and 1.02 eV for $(Ba_{0.8}Sr_{0.2})(Ti_{1-x}Zr_x)O_3$.[20,21] Thus, the calculated $E_a$ is acceptable.

A summary of the dielectric properties between 1 kHz and 1 MHz from −160 °C to 200 °C for $Dy_3NbO_7$ is shown in Fig. 8. The real part of the relative permittivity is between 34 and 39, and the imaginary part of the relative permittivity is on the order

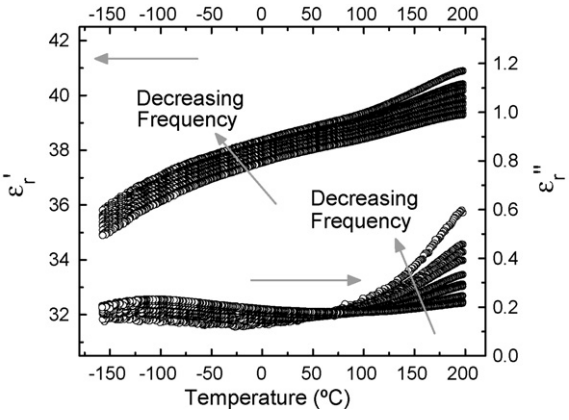


Fig. 8. Real and imaginary part of the relative permittivity of $Dy_3NbO_7$ at 1 kHz, 4 kHz, 6 kHz, 10 kHz, 30 kHz, 80 kHz, 100 kHz, 300 kHz, 800 kHz and 1 MHz.

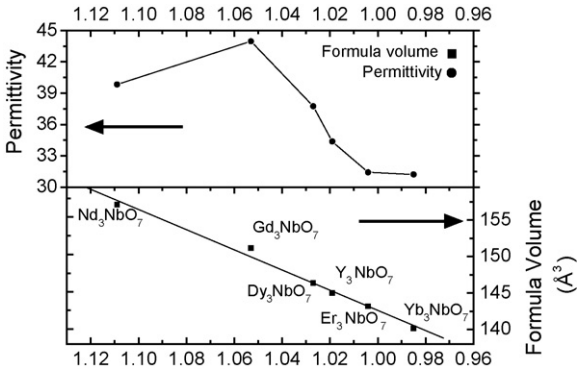


Fig. 9. Relative permittivity (room temperature and 1 MHz) and formula volume for $Ln_3NbO_7$.

of $10^{-1}$ at 1 MHz from −160 °C to 200 °C and slightly with decreasing measuring frequency. The positive temperature coefficient of the real part of the relative permittivity shows two slope variations (inflection points) with associated changes in the imaginary part with a peculiar cross-over at approximately 80 °C. The dielectric properties of $Er_3NbO_7$, $Yb_3NbO_7$ and $Y_3NbO_7$ show the same trend as that of $Dy_3NbO_7$. The room temperature real part of the relative permittivity is 31.4, 31.2 and 34.7 for $Er_3NbO_7$, $Yb_3NbO_7$ and $Y_3NbO_7$, respectively, and the imaginary part is on the order of $10^{-1}$ from −160 °C to 200 °C at 1 MHz. All of the compounds have positive TCCs, which are around 350 ppm/°C.

When the observed dielectric constants for these compounds are compared with the predicted values using the Clausius–Mosotti equation, the calculated values only account for 50% of the experimentally observed dielectric constants. It is important to note that the Clausius–Mosotti equation is derived under the assumption that ions of one type are symmetrically arranged around ions of another type.[22] As such, the equation is used to estimate the dielectric constants contributed by electronic and ionic mechanism with the calculated values agreeing well for the majority of non-polar inorganic oxides.[13] The large deviation of $\varepsilon'_{cal}$ from $\varepsilon'_{obs}$ indicates that the assumption may not hold for defect fluorite structures because of unoccupied oxygen sites and the double occupancy of the lanthanide ions in both A and B sites. It may also suggest that there exists a weak dipolar contribution contributing to the permittivity in these compounds.

A summary of the real part of the relative permittivity of $Ln_3NbO_7$ at room temperature and 1 MHz is shown in Fig. 9. While it can be expected that the more polarizable $Ln^{3+}$ ions result in higher permittivity, but $Gd_3NbO_7$ is an exception. It has higher dielectric permittivity than that of $Nd_3NbO_7$, even though the polarizability of $Gd^{3+}$ is lower than that of $Nd^{3+}$. Sirotinkin et al.[3] revealed an abnormally loose structure in $Ln_3NbO_7$ compounds in the middle of the series (Sm, Eu and Gd). According to the lattice parameters calculated in this work, $Gd_3NbO_7$ has the highest ratio of the formula volume (unit cell volume/formula number) to the $Ln^{3+}$ ionic radius (Fig. 9). It is predicted that the "looseness" increases the probability of polar distortions of these structures.[15] These polar distortions may be responsible for both high dielectric constant and abnormal dielectric response compared to other $Ln_3NbO_7$.

In addition, it is worth noting the possibility of forming $Ln_2(Ln',Nb)O_7$ pyrochlores, where the ionic radius of $Ln'^{3+}$ is smaller than that of $Ln^{3+}$.[2] It would be interesting to investigate these compounds to gain better understanding on dielectric behavior of fluorite-related structures.

## 4. Conclusion

The series of $Ln_3NbO_7$ (Ln = Nd, Gd, Dy, Er, Yb and Y) were successfully synthesized by solid-state processing. The crystal structure with increasing ionic radius changes from a defect cubic fluorite to orthorhombic weberite-type structures. The dielectric properties were also investigated. The experimentally determined room temperature dielectric constants are 30–45 at 1 MHz. The three different structures show different dielectric property behavior as a function of temperature. The real part of the relative permittivity of $Ln_3NbO_7$ (Ln = Nd, Dy, Er, Yb and Y) increases with increasing temperature, with $Nd_3NbO_7$ doing so at a higher rate than the other compounds. $Gd_3NbO_7$ demonstrates dielectric relaxation behavior. The calculated attempt frequency is $3.6675 \times 10^{11}$ Hz and the activation energy is 0.4518 eV.

## Acknowledgements

The authors would like to thank Josh Mangum for assisting the SEM investigation at the Major Analytical Instrumentation Center (MAIC) at the University of Florida, and the financial support by the U.S. National Science Foundation for funding CAREER grant (DMR-0449710).

## References

1. Subramanian, M. A., Aravamudan, G. and Rao, G. V. S., Oxide pyrochlores—a review. *Prog. Solid State Chem.*, 1983, **15**, 55–143.
2. Isupov, V. A., Oxide pyrochlores and their phase transition. *Ferroelectr. Rev.*, 2000, **2**, 115–168.
3. Sirotinkin, V. P., Evdokimov, A. A. and Trunov, V. K., Parameter improvement of nucleus of $Ln_3NbO_7$ and $Ln_3TaO_7$ compounds. *Zh. Neorg. Khim.*, 1982, **27**, 1648–1652.
4. Rossell, H. J., Fluorite-related phases $Ln_3MO_7$, Ln = rare-earth, Y or Sc, M = Nb, Sb, or Ta. 2. Structure determination. *J. Solid State Chem.*, 1979, **27**, 115–122.
5. Allpress, J. G. and Rossell, H. J., Fluorite-related phases $Ln_3MO_7$, Ln = rare-earth, Y, or Sc, M = Nb, Sb, or Ta. 1. Crystal-chemistry. *J. Solid State Chem.*, 1979, **27**, 105–114.
6. Rooksby, H. P. and White, E. A. D., Rare-earth niobates and tantalates of defect fluorite-type and weberite-type structures. *J. Am. Ceram. Soc.*, 1964, **47**, 94–96.
7. Thakre, O. B., Patil, P. V. and Chinchol, Vs., Crystallographic studies in system $(1-X)La_3NbO_7 + XSm_3NbO_7$. *Curr. Sci.*, 1971, **40**, 62.
8. Abe, R., Higashi, M., Zou, Z. G., Sayama, K., Abe, Y. and Arakawa, H., Photocatalytic water splitting into $H_2$ and $O_2$ over $R_3TaO_7$ and $R_3NbO_7$ (R = Y, Yb, Gd, La): effect of crystal structure on photocatalytic activity. *J. Phys. Chem. B*, 2004, **108**, 811–814.
9. Kovyazina, S. A., Perelyaeva, L. A., Leonidov, I. A. and Bakhteeva, Y. A., High-temperature structural disorder in $R_3NbO_7$. *J. Struct. Chem.*, 2003, **44**, 975–979.
10. Vente, J. F., Helmholdt, R. B. and Ijdo, D. J. W., The structure and magnetic-properties of $Pr_3MO_7$ with M = Nb, Ta, and Sb. *J. Solid State Chem.*, 1994, **108**, 18–24.

11. Yakubovich, O., Urusov, V., Massa, W., Frenzen, G. and Babel, D., Structure of $Na_2Fe_2F_7$ and structural relations in the family of weberites $Na_2M^{ii}M^{iii}F_7$. *Z. Anorg. Allg. Chem.*, 1993, **619**, 1909–1919.
12. Shannon, R. D., Revised effective ionic-radii and systematic studies of interatomic distances in halides and chalcogenides. *Acta Crystallogr. Sect. A*, 1976, **32**, 751–767.
13. Shannon, R. D., Dielectric polarizabilities of ions in oxides and fluorides. *J. Appl. Phys.*, 1993, **73**, 348–366.
14. Chinchol, Vs., Dielectric constants of system $XSm_3NbO_7 + (1 - X)La_3NbO_7$. *Curr. Sci.*, 1971, **40**, 400.
15. Astafyev, A. V., Sirotinkin, V. P. and Stefanovich, S. Y., Phase-transitions in the compounds $Sm_3NbO_7$ and $Gd_3NbO_7$ with a fluorite-like structure. *Kristallografiya*, 1985, **30**, 603–604.
16. Yokogawa, Y., Yoshimura, M. and Somiya, S., Lattice energy and polymorphism of fluorite-related rare earth-tantalum double oxides. *Solid State Ionics*, 1989, **35**, 275–279.
17. Wakeshima, M., Nishimine, H. and Hinatsu, Y., Crystal structures and magnetic properties of rare earth tantalates $RE_3TaO_7$ (RE = rare earths). *J. Phys.-Condens. Matter*, 2004, **16**, 4103–4120.
18. Elissalde, C., Ravez, J. and Gaucher, P., Dielectric relaxations in ceramics with compositions $(1 - X)Pb(Mg_{1/3}Nb_{2/3})O_3 - XPbTiO_3$ ($X = 0$, 0.05, 0.10 and 0.25). *Mater. Sci. Eng. B-Solid State Mater. Adv. Technol.*, 1994, **22**, 303–309.
19. Bokov, A. A., Leshchenko, M. A., Malitskaya, M. A. and Raevski, I. P., Dielectric spectra and Vogel–Fulcher scaling in $Pb(In_{0.5}Nb_{0.5})O_3$ relaxer ferroelectric. *J. Phys.-Condens. Matter*, 1999, **11**, 4899–4911.
20. Johnson, H. B., Tolar, N. J., Miller, G. R. and Cutler, I. B., Electrical and mechanical relaxation in $CaF_2$ doped with NaF. *J. Phys. Chem. Solids*, 1969, **30**, 31–42.
21. Cheng, B. L., Wang, C., Wang, S. Y., Button, T. W., Lu, H. B., Zhou, Y. L., Chen, Z. H. and Yang, G. Z., Temperature stability of permittivity and dielectric relaxation in multilayered thin films of $(Ba_{0.80}Sr_{0.20})(Ti_{1-x}Zr_x)O_3$ with a compositionally graded layer. *Appl. Phys. Lett.*, 2004, **84**, 5431–5433.
22. Roberts, S., Dielectric constants and polarizabilities of ions in simple crystals and barium titanate. *Phys. Rev.*, 1949, **76**, 1215–1220.